

Influence of Dye-Coordinated Metal Ions on Electron Transfer Dynamics at Dye–Semiconductor Interfaces

Omotola O. Ogunsolu,[†] Alexander J. Braun,[‡] Alex J. Robb,[‡] Sahan R. Salpage,[‡] Yan Zhou,[‡] and Kenneth Hanson^{*,†,‡}

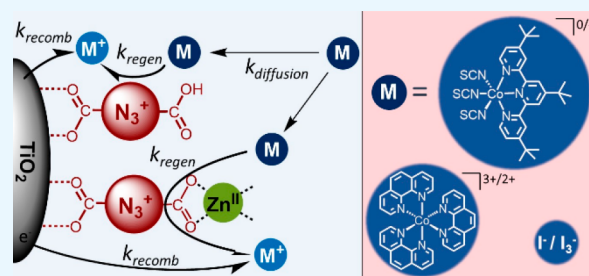
[†]Materials Science & Engineering, Florida State University, Tallahassee, Florida 32310, United States

[‡]Department of Chemistry & Biochemistry, Florida State University, Tallahassee, Florida 32306, United States

S Supporting Information

ABSTRACT: Maximizing regeneration and minimizing recombination rates at dye–semiconductor interfaces is crucial for the realization of efficient dye-sensitized solar and photoelectrosynthesis cells. Previously it has been shown that simply coordinating the metal ion to the nonsurface bound carboxylate groups of a dye molecule can slow recombination rates and increase open-circuit voltages. However, it was unclear if the additional steric effects or charge of the metal ion were the cause of this behavior. Here we use three different redox mediators, (1) I^-/I_3^- , (2) [tris(1,10-phenanthroline)cobalt]^{3+/2+}, and (3) [Co(4,4',4''-trityl-butyl-2,2':6',2''-terpyridine)(NCS)₃]^{0/1-} to elucidate the role, if any, of electrostatic interactions between the coordinated metal ion and mediator in dictating these interfacial electron transfer events. Using a combination of spectroscopy, electrochemistry, and solar cell measurements, we demonstrate that while electrostatic interactions may influence dye regeneration rates, for example, increased steric bulk of the metal ion between TiO₂(e⁻) and the oxidized mediator likely has a stronger influence on the overall device performance. Additionally, electrochemical impedance spectroscopy and intensity dependent measurements suggest that the coordination of the metal ion can slow diffusion of the mediators within the mesoporous oxide which could have implications for the use of multilayer assemblies in dye-sensitized devices.

KEYWORDS: electron transfer, kinetics, regeneration, redox mediator, dye-sensitized solar cells



INTRODUCTION

The rate of electron transfer at electrolyte–dye–metal oxide interfaces is a critical factor dictating the efficiency of photocurrent and solar fuels generation in dye-sensitized solar cells (DSSCs) and dye-sensitized photoelectrosynthesis cells (DSPECs), respectively.^{1–3} For both device architectures, excitation of the dye (k_{ex}) is followed by electron injection (k_{inj}) into the metal oxide and the buildup of one or more redox equivalents in the surface bound molecules (Figure 1). In an idealized cell, the oxidized dye (or catalyst in a DSPEC) is then reduced (k_{regen}) by the redox mediator (substrate) and the injected electron can enter the external circuit to generate power and close the circuit (reduce substrate).

In addition to the productive processes (i.e., k_{ex} , k_{inj} , k_{regen} , and k_{red}), there are several competitive, nonproductive events including back electron transfer from the metal oxide to the oxidized dye (k_{bet}) or mediator/substrate (k_{recomb}). Inhibiting the loss pathways and maximizing the rate of productive processes are key to realizing high efficiency devices. This is particularly true for water oxidation DSPECs where four oxidative equivalents must be built up and catalysis must occur faster than k_{bet} and k_{recomb} .^{4–7} The diffuse nature of solar energy (100 mW/cm²) results in approximately one excitation event per dye per second and thus k_{bet} and k_{recomb} must be slowed

to the order of 1 s⁻¹ time scales.^{2,8} Thus, new strategies are needed to influence and control electron transfer rates at dye–semiconductor–electrolyte interfaces.⁹

Our group introduced metal ion linked self-assembled bilayers¹⁰ of complementary chromophores as a means of not only broadening light absorption but also inhibiting k_{bet} and k_{recomb} by increasing the spatial separation between the metal oxide and the oxidized dye and/or redox mediator.¹¹ Interestingly, even without the second chromophore, simply coordinating the metal ion to the dye molecule monolayer resulted in an increase in open-circuit voltage (V_{oc}) by >30 mV. To understand the origin of this behavior, we initiated a systematic study of a photoanode composed of N3 dye functionalized TiO₂ (TiO₂–N3 in Figure 1b) coordinated with eight different metal ions and with iodide/triiodide (I^-/I_3^-) as the redox mediator.¹² The metal ion coordination had minimal influence on the photophysical and electrochemical properties of the N3 dye; however there was a general, but not

Special Issue: New Chemistry to Advance the Quest for Sustainable Solar Fuels

Received: September 14, 2018

Accepted: November 6, 2018

Published: November 19, 2018

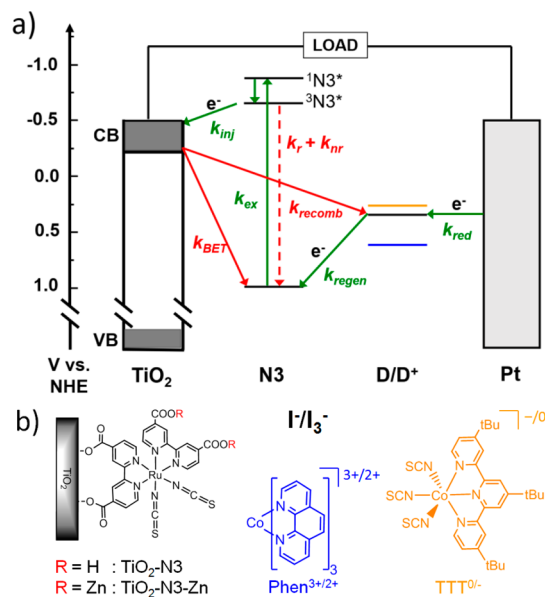


Figure 1. (a) Dynamic events, energetics (vs NHE) of TiO₂, N3, and the mediators (D/D⁺) with productive and nonproductive processes in green and red, respectively, and (b) schematic representation of TiO₂-N3, TiO₂-N3-Zn, and I⁻/I₃⁻, Phen^{3+/2+}, and TTT^{0/-} mediators (k_{ex} = excitation, k_r = radiative decay, k_{nr} = nonradiative decay, k_{inj} = electron injection, k_{bet} = back electron transfer, k_{regen} = regeneration, k_{recomb} = recombination, k_{red} = mediator reduction).

universal, trend of decreasing short-circuit current (J_{sc}) and increasing V_{oc} by up to 130 mV, with decreasing charge of the metal ion ($\text{M}^{\text{IV}} \rightarrow \text{M}^{\text{III}} \rightarrow \text{M}^{\text{II}}$). The lack of trend with respect to radius or coordination number of the metal ion suggested that electrostatic interactions between the metal ion and the I⁻/I₃⁻ mediator were responsible for the observed behavior.

Concurrently, Meyer and co-workers reported a system intentionally designed to facilitate electrostatic interactions between the dye and the redox mediator.¹³ They observed strong ion-pairing between the cationic tetraalkylammonium functionalized dye and the anionic [Co(4,4',4''-trityl-2,2':6',2''-terpyridine)(NCS)₃]⁻ mediator (TTT^{0/-}) which dramatically increased k_{regen} relative to a cationic mediator. With these results in mind, if an electrostatic interaction is responsible for the slowed k_{regen} and k_{recomb} in the TiO₂-N3-M^(II/III/IV) system, then in addition to changes in the metal ion, the electron transfer rates should also be influenced by the charge of the redox mediator. To test this hypothesis, here we study the device performance and electron transfer rates for TiO₂-N3 and TiO₂-N3-Zn in the presence of three different redox mediators: (1) iodide/triiodide (I⁻/I₃⁻) with negative charge in both the reduced and oxidized states, (2) [tris(1,10-phenanthroline)cobalt]^{3+/2+} (Phen^{3+/2+} in Figure 1a) with both states having a positive charge, and (3) TTT^{0/-} having a neutral in the oxidized form but negative in the reduced form. We use a combination of spectroscopy, electrochemistry, and solar cell measurements to probe k_{bet} , k_{regen} , k_{recomb} , k_{red} , and mediator diffusion coefficients. Collectively these results show that while electrostatic interactions may influence some of these events in TiO₂-N3-Zn relative to TiO₂-N3, its role is limited and the overall device performance is more strongly influenced by the additional steric effect provided by the coordinated metal ion.

EXPERIMENTAL SECTION

Materials. TiO₂ paste (18 NR-T) and ruthenium(II) *cis*-bis-(isothiocyanato)-bis(2,2'-bipyridyl-4,4'-dicarboxylic acid) (N3) were purchased and used as received from Dyesol and Solaronix, respectively. TTT^{0/-},^{13,14} and Phen^{3+/2+},¹⁶ were prepared following previously published procedures. Fluorine-doped tin oxide (FTO) glass substrates were purchased from Hartford Glass Co. (sheet resistance, 15 Ω □⁻¹). Iodine (I₂, Fisher Scientific), 1-butyl-3-methylimidazolium iodide (BMII, Aldrich), 4-*tert*-butylpyridine (TBP, Aldrich), dihydrogen hexachloroplatinate(IV) hexahydrate (H₂PtCl₆·6H₂O, Alfa Aesar), nitrosyl tetrafluoroborate (NOBF₄, Aldrich), 1,10-phenanthroline (Aldrich), titanium tetrachloride (TiCl₄, Fluka), tetrabutylammonium thiocyanate ((TBA)NCS, Aldrich), cobalt(II) chloride hexahydrate (CoCl₂·6H₂O, Aldrich), 4,4',4''-trityl-2,2':6',2''-terpyridine (TTT, Aldrich), zinc(II) acetate dihydrate (Zn(CH₃COOH)₂·2H₂O, Alfa Aesar), acetonitrile (Aldrich), acetone (Aldrich), methanol (Aldrich), and ethanol (EtOH, Koptec) were all used as purchased without further purification.

Film Preparation. FTO glass substrates were sonicated in ethanol and then HCl/Ethanol (15/85% mix) for 20 min. These were immersed in ~80 mM aqueous TiCl₄ solution at 70 °C for 30 min, rinsed with water, and sintered at 500 °C for 30 min. Nanocrystalline TiO₂ films ~5 μm thick, coating an area of 7 × 7 mm² on top of TiCl₄ treated FTO glass, were prepared by screen printing Dyesol 18 NR-T TiO₂ paste with an ATMA screen printer and subsequently sintered at 500 °C for 30 min. The screen printed TiO₂ film was again treated with ~40 mM aqueous TiCl₄ solution, rinsed with water, and sintered at 500 °C for 30 min. TiO₂-N3 film was prepared by soaking the TiO₂ thin film in a 0.4 mM ethanol solution of N3 dye. The slides were then removed after 24 h, rinsed with MeCN, and dried under a stream of air. TiO₂-N3-Zn film was prepared by immersing the TiO₂-N3 film in 0.5 mM solution of zinc metal acetate salt in methanol for 2 h. The slides were rinsed with MeCN and dried under a stream of air.

DSSC Fabrication. The functionalized TiO₂ films (TiO₂-N3 and TiO₂-N3-Zn) on FTO glass (1.4 × 1.9 cm²) served as the photoanode of the DSSCs. The cathode was prepared by first drilling a small hole ($d = 1.1$ mm) into the corner of the 2.0 × 2.2 cm² glass slide. The drilled slides were thereafter sonicated with ethanol for 10 min. This was followed by deposition of platinum by drop casting 75 μL of a ~4 mM solution of H₂PtCl₆ in ethanol on FTO glass followed by heat treatment (400 °C) using a Leister hot air blower. DSSC sandwich cells were prepared using a home-built assembly apparatus.^{11,17} A 2 mm wide 1.2 × 1.2 cm² Surlyn thermoplastic (25 μm thick Meltonix 1170-25 from Solaronix) was placed between the anode and the cathode and the entire ensemble heated to ~150 °C for 7 s. The electrolyte was introduced into the cell through a hole on the counter electrode using vacuum back-filling. Three electrolyte formulations, all in acetonitrile solvent, were used, namely,

I ⁻ /I ₃ ⁻ :	0.1 M BMII, 0.01 M I ₂ , 0.1 M TBP
Phen ^{3+/2+} :	0.1 M Co(II), 0.01 M Co(III), 0.1 M TBP
TTT ^{0/-} :	0.1 M Co(II), 0.01 M Co(III), 0.1 M TBP

The cell was then sealed by heating a meltonix film and a 4 × 4 mm² portion of a micro cover glass slide (18 × 18 mm² VWR).

Film and Device Characterization. Attenuated total reflectance infrared absorption, UV/vis absorption, nanosecond transient absorption, photocurrent density-voltage curves, incident photon-to-current efficiency and electrochemical impedance spectroscopy measurements were performed as previously reported.^{12,17} Details of these procedures are reported in the Supporting Information.

Diffusion Coefficients. Mediator diffusion coefficients were determined using previously published procedures.^{15,18} Briefly, cyclic voltammetry measurements (CHI-630E) were performed on 0.1 M (TBA)PF₆ solutions containing I⁻, Phen²⁺, or TTT⁻ at a scan rate of 0.01 V/s using a platinum working microelectrode (CHI108; 25 μm diameter active area), a platinum wire counter electrode, and a silver wire reference electrode. Diffusion coefficients (D , cm²/s) were then determined using $I_{\text{lim}} = 4nFDc$, where I_{lim} is the plateau current for the oxidative scan, n is the number of electrons exchanged per molecule (n

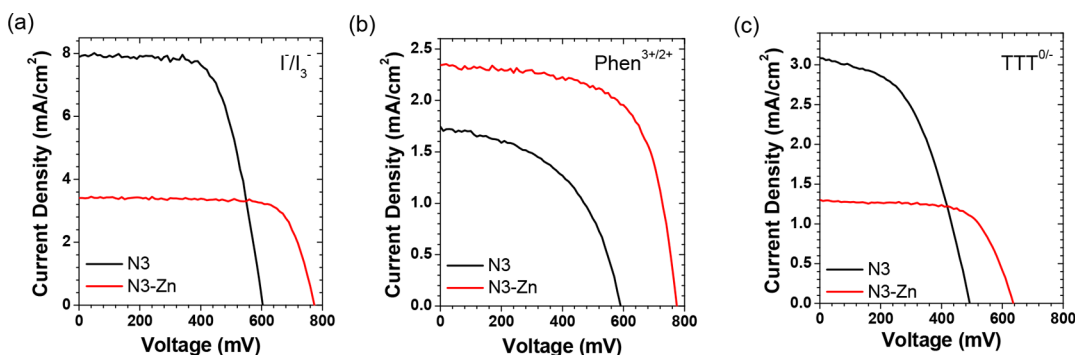


Figure 2. Photocurrent density–voltage (J – V) curves for DSSCs with photoanodes composed of TiO_2 –N3 and TiO_2 –N3–Zn with (a) I^-/I_3^- , (b) $\text{Phen}^{3+/2+}$, and (c) $\text{TTT}^{0/-}$ redox mediators.

Table 1. Performance Characteristics of DSSCs Containing TiO_2 –N3 and TiO_2 –N3–Zn Photoanodes with I^-/I_3^- , $\text{Phen}^{3+/2+}$, and $\text{TTT}^{0/-}$ Redox Mediators^a

		J_{sc} (mA/cm ²)	V_{oc} (mV)	FF (%)	η (%)
TiO_2 –N3	I^-/I_3^-	7.85 ± 0.11	610 ± 15	67 ± 0.40	3.20 ± 0.11
	$\text{Phen}^{3+/2+}$	1.75 ± 0.01	580 ± 20	49 ± 2.76	0.50 ± 0.04
	$\text{TTT}^{0/-}$	3.13 ± 0.18	490 ± 5	50 ± 2.31	0.76 ± 0.07
TiO_2 –N3–Zn	I^-/I_3^-	3.85 ± 0.93	770 ± 10	75 ± 2.11	2.20 ± 0.47
	$\text{Phen}^{3+/2+}$	2.37 ± 0.15	760 ± 15	66 ± 1.82	1.96 ± 0.15
	$\text{TTT}^{0/-}$	1.26 ± 0.15	620 ± 30	67 ± 1.96	0.52 ± 0.04

^aAll data are the average value from the measurement of three separate DSSCs and the error (\pm) are the standard deviation of those measurements.

= 1), F is Faraday's constant (96485 CS/mol), C is concentration of solute (0.0001 mol/cm³), and r is the radius of the working electrode (12.5 μm).

Intensity Dependence. Photocurrent density vs excitation power density plots were recorded using a CH Instruments CHI630E electrochemical analyzer. Sandwich cell samples were prepared as described above and were composed of a TiO_2 –N3 or TiO_2 –N3–Zn working electrode, a platinum counter electrode, and the three electrolyte solutions. The samples were irradiated with 532 nm light from a Nd:YAG laser (Aixiz, AD-532-400T) passed through a 2 mm diameter iris (Newport ID-1.0) and then directed to the sample via mirror. The intensity was controlled using a variable neutral density filter (Edinburgh F-B01 laser mount).

RESULTS AND DISCUSSION

Film Preparation. TiO_2 –N3–Zn films were composed of nanocrystalline titanium oxide (TiO_2), $\text{Ru}(4,4'-(\text{COOH})_2\text{bpy})_2(\text{NCS})_2$ (N3) dye, and a zinc(II) acetate dihydrate (Zn) and were prepared using a stepwise soaking procedure and monitored by UV–vis and ATR–IR spectroscopy.^{17,19,20} Upon zinc treatment, there was minimal shift (<20 nm) in the UV–vis absorption features of N3 (Supporting Information Figure S1).¹² However, the disappearance of the noncoordinated C=O stretch at $\sim 1720\text{ cm}^{-1}$ and an increase in the bipyridyl and COO peaks between ~ 1300 and 1700 cm^{-1} (Figure S2) are indicative of Zn(II) coordination to the nonsurface bound carboxylate groups of N3.¹² It is worth noting that due to a small degree of mobility of the N3 dye on the surface, one could envision that the addition of Zn^{II} ions could result in cross-surface N3–Zn–N3 coordination networks. We are currently unable to confirm or rule out such structures, but if they do form, they have minimal influence on the redox or spectroscopic properties of N3.

J – V Curves. Dye-sensitized solar cells were assembled with TiO_2 –N3 or TiO_2 –N3–Zn photoanodes, a platinum cathode, and an electrolyte composed of the 0.1 M/0.01 M redox mediators (I^-/I_3^- , $\text{Phen}^{3+/2+}$, and $\text{TTT}^{0/-}$) in a 0.1 M *tert*-

butylpyridine MeCN solution. The ratio and amount of mediator as well as the TBP additives were kept constant to mitigate concerns related to concentration. Photocurrent density–voltage (J – V) measurements were performed, and the results are summarized in Figure 2, Figure S3, and Table 1.

For both TiO_2 –N3 and TiO_2 –N3–Zn devices, the V_{oc} increases in the order $\text{TTT}^{0/-} < \text{Phen}^{3+/2+} < \text{I}^-/\text{I}_3^-$. In a DSSC, the maximum V_{oc} is dictated by the energy difference between the quasi Fermi level of the electrons within TiO_2 and potential of the redox mediator.²¹ As expected, given its relatively low oxidation potential ($E_{1/2}^{ox} = 0.27\text{ V}$ vs NHE),¹³ devices with $\text{TTT}^{0/-}$ gave a >100 mV lower V_{oc} than the other mediators. Interestingly, despite having a >200 mV more positive potential, the V_{oc} for the $\text{Phen}^{3+/2+}$ ($E_{1/2}^{ox} = 0.62\text{ V}$)^{15,22} devices was comparable to I^-/I_3^- (0.35 V).^{2,22} This signals that the Fermi level of electrons in TiO_2 is $\sim 200\text{ mV}$ lower for the $\text{Phen}^{3+/2+}$ than I^-/I_3^- . The Fermi level, and resulting V_{oc} , is dictated by the ratio between the rate of electrons entering ($\text{Rate}_{e^- \text{ in}}$) and exiting ($\text{Rate}_{e^- \text{ out}}$) the metal oxide as described by the modified diode equation (eq 1):

$$V_{oc} \propto \frac{k_B T}{e} \ln \left(\frac{\text{Rate}_{e^- \text{ in}}}{\text{Rate}_{e^- \text{ out}}} \right) \quad (1)$$

where k_B is the Boltzmann constant, T is the temperature, and e is the elementary charge.¹ Since k_{inj} is ultrafast^{23,24} and assumed to be similar regardless of the mediator, the lower V_{oc} for $\text{Phen}^{3+/2+}$ compared to I^-/I_3^- can be attributed to either a slower k_{regen} , faster k_{bet} , and/or faster k_{recomb} . For the TiO_2 –N3–Zn film, although the trend in k_{regen} could be rationalized by an electrostatic interaction ($k_{regen(\text{Phen}^{2+})} < k_{regen(\text{I}^-)}$), a faster k_{recomb} is contrary to the expectation that the N3–Zn– Phen^{3+} interaction is less favorable than N3–Zn– I_3^- . This discrepancy, combined with the similarity in trends for both TiO_2 –N3 and TiO_2 –N3–Zn, suggest that the charge of the metal ion does not play as critical a role as we previously proposed.

When comparing the films without and with metal ion treatment (Figure 2), there is an increase in V_{oc} by >100 mV regardless of the nature of the mediator. Previously, we demonstrated that acetic acid or acetate treatments of TiO_2 -N3 had minimal influence on the device performance,¹² strongly indicating that metal ion coordination is responsible for the change. The increased V_{oc} was attributed to the metal ion increasing the steric bulk between $TiO_2(e^-)$ and the oxidized mediator effectively slowing k_{recomb} .^{11,12} Given that the trend and magnitude of the change in V_{oc} is similar regardless of the mediator, it again suggests that any electrostatic interaction plays a diminished role in dictating the electron transfer dynamics at this interface.

For both I^-/I_3^- and $TTT^{0/-}$ there is a dramatic decrease in J_{sc} upon metal ion coordination that would not be expected if N3-Zn... I^- and N3-Zn... TTT^- electrostatic interactions were strongly favoring k_{regen} as previously observed in the system reported by Meyer and co-workers.¹³ A decrease in injection yield upon metal ion coordination¹² can account for some of the decrease, but the more than 2-fold decrease in J_{sc} must be due to slower k_{regen} and/or faster k_{recomb} .

Electrochemical Impedance Spectroscopy. To gain insights into the electron transfer dynamics in operational devices, we performed electrochemical impedance spectroscopy. The measurement was conducted on the sandwich cells at open-circuit voltage under AM 1.5 irradiation (100 mW/cm²), and the results are shown as a Nyquist plot in Figure 3. The curves in Figure 3 were fit to an equivalent circuit (Figure S5) previously reported by Bisquert and co-workers,²⁵⁻²⁷ and the results are summarized in Table S1 and Figure S6.

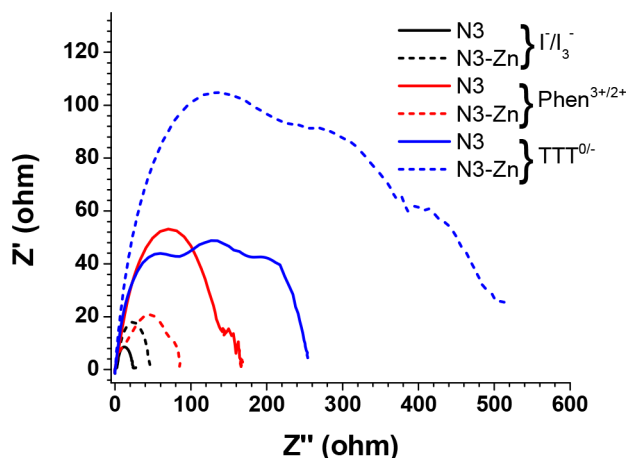


Figure 3. Nyquist plot for DSSCs with TiO_2 -N3 and TiO_2 -N3-Zn photoanodes and I^-/I_3^- , $Phen^{3+/2+}$, and $TTT^{0/-}$ redox mediators.

Nyquist plots for DSSCs are generally composed of three arcs, from 1 MHz to ~0.1 Hz (left to right in Figure 3), that correspond to (1) the charge transfer at the cathode-electrolyte interface, (2) the charge transfer resistance at the electrolyte-dye- TiO_2 interface, and (3) diffusion through the electrolyte.²⁷⁻³⁰ For a typical liquid electrolyte DSSC containing I^-/I_3^- redox mediator in nitrile solvents, the first and second arcs are observed with the latter being the dominant feature. The small size of the first arc is typically due to the low resistance for I_3^- reduction at the cathode^{18,30,31} while the third arc is either not observable or appears as a small shoulder because of the fast diffusion of I^-/I_3^- through the solvent.^{25,27} These characteristic

features can be seen in Figure 3 for the TiO_2 -N3 and TiO_2 -N3-Zn devices with I^-/I_3^- (black solid and dashed lines).

In contrast, for the cobalt containing electrolytes, $Phen^{3+/2+}$ and $TTT^{0/-}$, there are two and three readily defined arcs, respectively. The observation of the third, low frequency arc indicates that diffusion through the solvent is slower for the cobalt mediators than iodide and in the TiO_2 -N3 device, for example, effective diffusivity (D_{eff}) decreases in the order I^-/I_3^- (7.6×10^{-4} cm²/s) > $Phen^{3+/2+}$ (5.8×10^{-4} cm²/s) > $TTT^{0/-}$ (0.3×10^{-4} cm²/s). This observation is in agreement with previous reports that the large size of the cobalt complexes (>10 Å), compared to I^- (~2 Å) or I_3^- (<5 Å), significantly hinders diffusion of the molecules through the solvent.^{22,32} Presumably the bulky tertbutyl groups on $TTT^{0/-}$ further hinder its mobility resulting in the highest diffusion resistance. Interestingly, of the three mediators, $TTT^{0/-}$ was the only one to exhibit a large charge transfer resistance at the cathode-electrolyte interface ($R_{Pt(N3)} = 81.8 \Omega$). This observation suggests that reduction of TTT^0 at platinum is a much slower process than for I_3^- or $Phen^{3+}$, which could be attributed to slower reaction kinetics for the electron transfer event.³³ Alternatively, since TTT^0 is the only neutral species of the three, one could envision an electrostatic charge at the cathode or a charged double layer may hinder contact between the mediator and the electrode.

For both I^-/I_3^- and $TTT^{0/-}$ devices, the charge transfer resistance at the electrolyte-dye- TiO_2 interface, (given by the diameter of the second arc) increases upon the addition of the coordinated zinc ion. This can most readily be seen by the increase in the injected electron lifetime (τ_{eff}) from 6.4 to 10.1 ms for I^-/I_3^- and from 10.1 to 12.8 ms for $TTT^{0/-}$. Since k_{bet} is similar for TiO_2 -N3 and TiO_2 -N3-Zn (vide infra), this observation is consistent with slowed k_{recomb} , again likely due to increased steric hindrance provided by the Zn ion, and is partially responsible for the increased V_{oc} upon the addition of zinc. Interestingly, for $Phen^{3+/2+}$, a decrease in charge transfer resistance was observed. The origin of this behavior is currently unclear to us.

Transient Absorption Spectroscopy. Transient absorption (TA) spectroscopy was performed to elucidate the rate of back electron transfer and dye regeneration rates with respect to the redox mediators. Briefly, a 5 ns, 480 nm pulse of light was used to excite TiO_2 -N3 and TiO_2 -N3-Zn films both with and without I^-/I_3^- , $Phen^{3+/2+}$, and $TTT^{0/-}$ redox mediators in an acetonitrile solution. The dye bleach and recovery were monitored at 535 nm with an example kinetic trace for TiO_2 -N3 with and without I^-/I_3^- shown in Figure 4 with the remaining traces in Figure S7. The single wavelength kinetics were fit with a biexponential function with the fitting values and calculated rate constants shown in Table 2 and Table S2.

In these experiments, excitation of TiO_2 -N3 and TiO_2 -N3-Zn is followed by sub-picosecond electron transfer from N3* to TiO_2 ^{34,35} and the generation of N3⁺ as indicated by a bleach ($-\Delta OD$) in the ground state absorption feature of N3 at 535 nm. In the absence of mediator, the bleach recovery is dominated by $TiO_2(e^-)$ to N3⁺ back electron transfer. As can be seen in Table 2, k_{bet} is similar for both TiO_2 -N3 (4.0×10^5 s⁻¹) and TiO_2 -N3-Zn (3.7×10^5 s⁻¹) indicating that Zn ion coordination has minimal influence on the back electron transfer kinetics. However, upon the addition of I^-/I_3^- , $Phen^{3+/2+}$, and $TTT^{0/-}$, the return to baseline is faster due to the mediator to N3⁺ electron transfer event (k_{regen}). Assuming the only difference in lifetimes between the two samples (with and

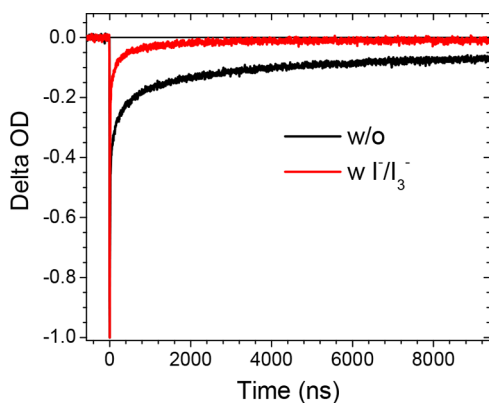


Figure 4. Transient absorption trace at 535 nm for $\text{TiO}_2\text{-N3}$ with and without I^-/I_3^- redox mediator in MeCN ($\lambda_{\text{ex}} = 480$ nm).

without mediator) is dye regeneration, then k_{regen} can be calculated using eqs 2–4:

$$k_{\text{bet}} = 1/\tau_{\text{w/o}} \quad (2)$$

$$k_{\text{bet}} + k_{\text{regen}} = 1/\tau_{\text{w}} \quad (3)$$

$$k_{\text{regen}} = (1/\tau_{\text{w}}) - (1/\tau_{\text{w/o}}) \quad (4)$$

where $\tau_{\text{w/o}}$ and τ_{w} are the N3^+ lifetime in the absence and presence of the redox mediators.^{36–38} The results of these calculations can be seen in Table 2.

For both $\text{TiO}_2\text{-N3}$ ($9.4 \times 10^5 \text{ s}^{-1}$) and $\text{TiO}_2\text{-N3-Zn}$ ($2.4 \times 10^5 \text{ s}^{-1}$), samples with I^-/I_3^- mediator exhibited a k_{regen} that was >3 times faster than those containing cobalt mediators. The driving force of N3 regeneration is higher for $\text{TTT}^{0/-}$ than for I^-/I_3^- by ~ 100 mV but has an order of magnitude lower k_{regen} . The dramatic disparity could be due to the difference in reorganization energies for electron transfer,³⁹ but since k_{regen} is dependent on both the electron transfer and through-pore diffusion rates, it could also be due to much slower diffusion of the cobalt complexes. Given the high excitation intensities used in these TA measurements, diffusion limited regeneration is expected to play a much larger role in dictating k_{regen} .⁴⁰ It is worth noting that due to the high photon flux, the rate constants determined by TA do not necessarily represent those under ambient solar flux (AM1.5).

For both I^-/I_3^- and $\text{Phen}^{3+/2+}$ there is a 4-fold decrease in the regeneration rate from $\text{TiO}_2\text{-N3}$ to $\text{TiO}_2\text{-N3-Zn}$. Given that both mediators have different charges, this observation again suggests that steric effects, and not electrostatics, play a critical role in dictating k_{regen} . Interestingly, for the $\text{TTT}^{0/-}$ mediator, k_{regen} slightly increases from $\text{TiO}_2\text{-N3}$ ($0.3 \times 10^5 \text{ s}^{-1}$) to $\text{TiO}_2\text{-N3-Zn}$ ($0.8 \times 10^5 \text{ s}^{-1}$). A similar, albeit much more

pronounced behavior was observed by Casarin et al.¹³ where a hexacationic dye $\text{TTT}^{0/-}$ mediator was electrostatically bound to the hexacationic dye. The lower charge as well as increased spatial separation between the dye and mediator for the metal ion coordination strategy reported here could be responsible for a weaker interaction and smaller differences in k_{regen} . However, the lack of increased k_{regen} for I^-/I_3^- in the presence of Zn again suggests that electrostatics plays a limited role.

Mediator Diffusion. Diffusion coefficients for the I^- , Phen^{2+} , and TTT^- in bulk acetonitrile, were determined using cyclic voltammetry (CV) following the methods of Feldt et al.¹⁵ Briefly, the plateau current (I_{lim}) was determined from slow scan (0.01 V/s) oxidative CV measurements of the mediators in 0.1 M (TBA)PF₆ MeCN solutions using a planar platinum working microelectrode (25 μm diameter). D was then calculated using $I_{\text{lim}} = 4nFDcR$, where n is the number of electrons ($n = 1$), F is Faraday's constant, C is the concentration of the mediator, and r is the radius of the working electrode. Using this method with $[\text{Co}(\text{phen})_3(\text{PF}_6)_2]^{2+}$, we obtained a diffusion coefficient, $8.4 \times 10^{-6} \text{ cm}^2/\text{s}$, that is in good agreement with the previously reported value, $9.0 \times 10^{-6} \text{ cm}^2/\text{s}$.¹⁵ Using the same methodology, D decreases in the order I^- ($20.8 \times 10^{-6} \text{ cm}^2/\text{s}$) > Phen^{2+} ($8.4 \times 10^{-6} \text{ cm}^2/\text{s}$) > TTT^- ($1.3 \times 10^{-6} \text{ cm}^2/\text{s}$) which inversely corresponds to the size of the molecules $\text{I}^- \ll \text{Phen}^{2+} < \text{TTT}^-$ and is the same as the trend found from electrochemical impedance spectroscopy.

Measuring photocurrent from the DSSC with respect to light intensity also offers a means of probing mediator diffusion limited device performance.^{32,41} With low intensity light, the DSSCs photocurrent is limited by the rate of excitation (k_{ex}). Under those conditions the photocurrent will increase linearly with photon flux. There is however an intensity threshold at which excitation is sufficiently fast that the device becomes rate limited by k_{regen} and k_{red} events and the photocurrent becomes intensity independent ($m = 0$). For $\text{TiO}_2\text{-N3}$ and $\text{TiO}_2\text{-N3-Zn}$ regardless of the mediator, the photocurrent was found to be linearly dependent up to four equivalent suns intensity ($4 \times \text{AM1.5}$). This observation suggests that while the diffusion rates may be different between the mediators; the pores in the TiO_2 are sufficiently large⁴⁰ that diffusion does not limit the DSSC performance under normal operational conditions (AM1.5).

To observe flux independent photocurrent, we increased the excitation intensity by using a 532 nm laser as the light source and the results can be seen in Figures 5 and S7. Given that k_{ex} is dependent on both excitation source intensity and the absorbance of the sample, we corrected the x -axis to excitation events per second (photon/second \times absorbance) to allow for more universal comparisons between samples with different absorbance intensities and spectra. With I^-/I_3^- and $\text{Phen}^{3+/2+}$, the photocurrent remained linear with flux even in the high

Table 2. Weighted Average Lifetimes with (τ_{w}) and without ($\tau_{\text{w/o}}$) I^-/I_3^- , $\text{Phen}^{3+/2+}$, and $\text{TTT}^{0/-}$, k_{bet} , and k_{regen} from Transient Absorption Measurements of $\text{TiO}_2\text{-N3}$ and $\text{TiO}_2\text{-N3-Zn}$ in a MeCN Solution of 0.1 M TBP ($\lambda_{\text{ex}} = 480$ nm, 5 mJ/pulse, $\lambda_{\text{abs}} = 535$ nm)

	$\tau_{\text{w/o}}$ (ns)	k_{bet} ($\times 10^5 \text{ s}^{-1}$)		τ_{w} (ns)	$k_{\text{bet}} + k_{\text{regen}}$ ($\times 10^5 \text{ s}^{-1}$)	k_{regen} ($\times 10^5 \text{ s}^{-1}$)
$\text{TiO}_2\text{-N3}$	2460	4.0	I^-/I_3^-	740	13.4	9.4
			$\text{Phen}^{3+/2+}$	1360	7.4	3.3
			$\text{TTT}^{0/-}$	2300	4.4	0.3
$\text{TiO}_2\text{-N3-Zn}$	2680	3.7	I^-/I_3^-	1620	6.2	2.4
			$\text{Phen}^{3+/2+}$	2360	4.2	0.5
			$\text{TTT}^{0/-}$	2220	4.5	0.8

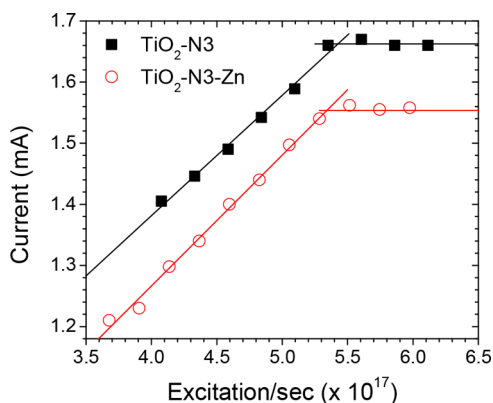


Figure 5. Photocurrent with respect to excitation rate for DSSCs containing $\text{TiO}_2\text{-N3}$ and $\text{TiO}_2\text{-N3-Zn}$ anodes and $\text{TTT}^{0/-}$ in MeCN.

intensity regimes (Figure S8), but a plateau was observed for $\text{TTT}^{0/-}$ based devices (Figure 5). This observation agrees with the trends in diffusion rates observed by EIS and CV measurements (vide supra), with $\text{TTT}^{0/-}$ being the slowest. However, given the anomalously large charge transfer resistance at the cathode–electrolyte interface for $\text{TTT}^{0/-}$, we cannot rule out k_{red} as the rate limiting step. Interestingly, the intensity of the current limiting threshold (I_{LT}), here defined as the intercept between linear fits of the two regions, was slightly large for $\text{TiO}_2\text{-N3}$ ($I_{\text{LT}} = 5.45 \times 10^{17}$ excitation/s) than $\text{TiO}_2\text{-N3-Zn}$ (5.30×10^{17} excitation/s). If this plateau and the I_{LT} value are dictated by mediator diffusion through the metal oxide pores, this could be rationalized as the metal ion coordination decreasing the pore diameter and reducing mediator mobility. While the zinc(II) ion itself is relatively small (0.88 Å), upon coordination to N3 it likely adopts a tetrahedral geometry with a N3 carboxylate group and acetate anion as the bidentate ligands. Using the van der Waals radii, we estimate that N3–Zn–OAc is approximately ~ 5 Å (N3 oxygen to acetate hydrogen distance) larger than N3 alone (~ 13 Å). Given pore diameters on the order of 20–30 nm, a 1 nm, or up to 5%, decrease in pore diameter is presumably enough to hinder the diffusion of larger redox mediators.

CONCLUSION

In this study we sought to determine the role that electrostatics and dye–metal ion coordination has on electron transfer at the dye–semiconductor–electrolyte interface. More specifically we used a combination of spectroscopy, electrochemistry, and solar cell measurements to probe k_{bet} , k_{regen} , k_{recomb} , k_{red} , and diffusion with respect to redox mediators having different charges (i.e., Γ^-/I_3^- , $\text{Phen}^{3+/2+}$, and $\text{TTT}^{0/-}$). For devices without ($\text{TiO}_2\text{-N3}$) and with metal ion coordination ($\text{TiO}_2\text{-N3-Zn}$) the trend in V_{oc} coincides with the redox potential of the mediator. However, despite having a >200 mV more positive redox potential, the V_{oc} for the $\text{Phen}^{3+/2+}$ device was comparable to Γ^-/I_3^- which can be attributed to the faster k_{regen} and slower k_{recomb} for Γ^-/I_3^- compared to $\text{Phen}^{3+/2+}$. While some observation such as $k_{\text{regen}}(\text{Phen}^{2+}) < k_{\text{regen}}(\Gamma^-)$ may be indicative of favorable electrostatic interactions between the mediator and metal ion, the effect is by no means dominating the device performance. For example, regardless of mediator, there was a > 100 mV increase in the V_{oc} upon metal ion coordination. Additionally, the trend and magnitude of the change in V_{oc} are similar and there is a general decrease in k_{recomb} upon metal ion coordination that are largely

independent of the charge of the mediator. Collectively these results suggest that the additional steric bulk between $\text{TiO}_2(\text{e}^-)$ and the oxidized mediator provided by the metal ion has a stronger influence on k_{regen} and k_{recomb} than does electrostatics. As a side, coordination of the metal ion does however appear to slow diffusion of the mediators within the mesoporous oxide as demonstrated by EIS and intensity dependent measurements. While the difference in diffusion may be small in this case, multilayer assemblies^{16,42–44} offer a promising means of broadening light absorption¹¹ and harnessing triplet–triplet annihilation⁴⁵ but, given their size, may also be limiting mediator diffusion within the pores. Work is currently underway in our laboratory to understand the role of pore diameter, metal ion coordination, and multilayer thickness on dye loading and inter-pore mobility.

ASSOCIATED CONTENT

Supporting Information

The Supporting Information is available free of charge on the ACS Publications website at DOI: 10.1021/acsam.8b01559.

Nanoparticle paste preparation, UV–vis, ATR–IR, device characterization, equivalent circuit, absorption spectra, and kinetic fits (PDF)

AUTHOR INFORMATION

Corresponding Author

*E-mail: hanson@chem.fsu.edu.

ORCID

Omotola O. Ogunsolu: 0000-0002-9446-3027

Yan Zhou: 0000-0002-7290-1401

Kenneth Hanson: 0000-0001-7219-7808

Notes

The authors declare no competing financial interest.

ACKNOWLEDGMENTS

This research was primarily supported by the Army Research Office under Grant No. W911NF-14-1-0660. Electrochemical diffusion measurements were supported by the National Science Foundation under Grant No. DMR-1752782. Transient absorption measurements were performed on a spectrometer supported by the National Science Foundation under Grant No. CHE-1531629.

REFERENCES

- (1) Ardo, S.; Meyer, G. J. Photodriven heterogeneous charge transfer with transition-metal compounds anchored to TiO_2 semiconductor surfaces. *Chem. Soc. Rev.* **2009**, *38*, 115–164.
- (2) Hagfeldt, A.; Boschloo, G.; Sun, L.; Kloo, L.; Pettersson, H. Dye-sensitized solar cells. *Chem. Rev.* **2010**, *110*, 6595–6663.
- (3) Ashford, D. L.; Gish, M. K.; Vannucci, A. K.; Brennaman, M. K.; Templeton, J. L.; Papanikolas, J. M.; Meyer, T. J. Molecular Chromophore-Catalyst Assemblies for Solar Fuel Applications. *Chem. Rev.* **2015**, *115*, 13006–49.
- (4) Brady, M. D.; Sampaio, R. N.; Wang, D.; Meyer, T. J.; Meyer, G. J. Dye-Sensitized Hydrobromic Acid Splitting for Hydrogen Solar Fuel Production. *J. Am. Chem. Soc.* **2017**, *139*, 15612–15615.
- (5) McCool, N. S.; Swierk, J. R.; Nemes, C. T.; Saunders, T. P.; Schmuttenmaer, C. A.; Mallouk, T. E. Proton-Induced Trap States, Injection and Recombination Dynamics in Water-Splitting Dye-Sensitized Photoelectrochemical Cells. *ACS Appl. Mater. Interfaces* **2016**, *8*, 16727–35.
- (6) Sheridan, M. V.; Wang, Y.; Wang, D.; Troian-Gautier, L.; Dares, C. J.; Sherman, B. D.; Meyer, T. J. Light-Driven Water Splitting Mediated

by Photogenerated Bromine. *Angew. Chem., Int. Ed.* **2018**, *57*, 3449–3453.

(7) Brennaman, M. K.; Gish, M. K.; Alibabaei, L.; Norris, M. R.; Binstead, R. A.; Nayak, A.; Lapides, A. M.; Song, W.; Brown, R. J.; Concepcion, J. J.; Templeton, J. L.; Papanikolas, J. M.; Meyer, T. J. Pathways Following Electron Injection: Medium Effects and Cross-Surface Electron Transfer in a Ruthenium-Based, Chromophore–Catalyst Assembly on TiO₂. *J. Phys. Chem. C* **2018**, *122*, 13017–13026.

(8) O'Regan, B. C.; Durrant, J. R. Kinetic and energetic paradigms for dye-sensitized solar cells: moving from the ideal to the real. *Acc. Chem. Res.* **2009**, *42*, 1799–808.

(9) Hamann, T. W.; Jensen, R. A.; Martinson, A. B. F.; Van Ryswyk, H.; Hupp, J. T. Advancing beyond current generation dye-sensitized solar cells. *Energy Environ. Sci.* **2008**, *1*, 66–78.

(10) Hanson, K.; Torelli, D. A.; Vannucci, A. K.; Brennaman, M. K.; Luo, H. L.; Alibabaei, L.; Song, W. J.; Ashford, D. L.; Norris, M. R.; Glasson, C. R. K.; Concepcion, J. J.; Meyer, T. J. Self-Assembled Bilayer Films of Ruthenium(II)/Polypyridyl Complexes through Layer-by-Layer Deposition on Nanostructured Metal Oxides. *Angew. Chem., Int. Ed.* **2012**, *51*, 12782–12785.

(11) Ogunsolu, O. O.; Murphy, I. A.; Wang, J. C.; Das, A.; Hanson, K. Energy and Electron Transfer Cascade in Self-Assembled Bilayer Dye-Sensitized Solar Cells. *ACS Appl. Mater. Interfaces* **2016**, *8*, 28633–28640.

(12) Ogunsolu, O. O.; Wang, J. C.; Hanson, K. Increasing the Open-Circuit Voltage of Dye-Sensitized Solar Cells via Metal-Ion Coordination. *Inorg. Chem.* **2017**, *56*, 11168–11175.

(13) Casarin, L.; Swords, W. B.; Caramori, S.; Bignozzi, C. A.; Meyer, G. J. Rapid Static Sensitizer Regeneration Enabled by Ion Pairing. *Inorg. Chem.* **2017**, *56*, 7324–7327.

(14) Benazzi, E.; Cristino, V.; Caramori, S.; Meda, L.; Boaretto, R.; Bignozzi, C. A. Electrochemical characterization of polypyridine iron(II) and cobalt(II) complexes for organic redox flow batteries. *Polyhedron* **2018**, *140*, 99–108.

(15) Feldt, S. M.; Gibson, E. A.; Gabrielsson, E.; Sun, L.; Boschloo, G.; Hagfeldt, A. Design of Organic Dyes and Cobalt Polypyridine Redox Mediators for High-Efficiency Dye-Sensitized Solar Cells. *J. Am. Chem. Soc.* **2010**, *132*, 16714–16724.

(16) Hill, S. P.; Hanson, K. Harnessing Molecular Photon Upconversion in a Solar Cell at Sub-solar Irradiance: Role of the Redox Mediator. *J. Am. Chem. Soc.* **2017**, *139*, 10988–10991.

(17) Ogunsolu, O. O.; Wang, J. C.; Hanson, K. Inhibiting Interfacial Recombination Events in Dye-Sensitized Solar Cells using Self-Assembled Bilayers. *ACS Appl. Mater. Interfaces* **2015**, *7*, 27730–4.

(18) Hauch, A.; Georg, A. Diffusion in the electrolyte and charge-transfer reaction at the platinum electrode in dye-sensitized solar cells. *Electrochim. Acta* **2001**, *46*, 3457–3466.

(19) Wang, J. C.; Violette, K.; Ogunsolu, O. O.; Hanson, K. Metal ion mediated electron transfer at dye-semiconductor interfaces. *Phys. Chem. Chem. Phys.* **2017**, *19*, 2679–2682.

(20) Wang, J. C.; Ogunsolu, O. O.; Sykora, M.; Hanson, K. Elucidating the Role of the Metal Linking Ion on the Excited State Dynamics of Self-Assembled Bilayers. *J. Phys. Chem. C* **2018**, *122*, 9835–9842.

(21) Nazeeruddin, M. K.; Baranoff, E.; Gratzel, M. Dye-sensitized solar cells: A brief overview. *Sol. Energy* **2011**, *85*, 1172–1178.

(22) Giribabu, L.; Bolligara, R.; Panigrahi, M. Recent Advances of Cobalt(II/III) Redox Couples for Dye-Sensitized Solar Cell Applications. *Chem. Rec* **2015**, *15*, 760–88.

(23) Benko, G.; Kallioinen, J.; Korppi-Tommola, J. E. I.; Yartsev, A. P.; Sundstrom, V. Photoinduced ultrafast dye-to-semiconductor electron injection from nonthermalized and thermalized donor states. *J. Am. Chem. Soc.* **2002**, *124*, 489–493.

(24) Wenger, B.; Grätzel, M.; Moser, J.-E. Rationale for Kinetic Heterogeneity of Ultrafast Light-Induced Electron Transfer from Ru(II) Complex Sensitizers to Nanocrystalline TiO₂. *J. Am. Chem. Soc.* **2005**, *127*, 12150–12151.

(25) Fabregat-Santiago, F.; Bisquert, J.; Garcia-Belmonte, G.; Boschloo, G.; Hagfeldt, A. Influence of electrolyte in transport and

recombination in dye-sensitized solar cells studied by impedance spectroscopy. *Sol. Energy Mater. Sol. Cells* **2005**, *87*, 117–131.

(26) Bisquert, J.; Fabregat-Santiago, F. Impedance Spectroscopy: A General Introduction And Application to Dye-Sensitized Solar Cells. *Dye-Sensitized Solar Cells*; CRC, Taylor and Francis: Boca Raton, FL, USA, 2010; Chapter 12, pp 1–99.

(27) Fabregat-Santiago, F.; Garcia-Belmonte, G.; Mora-Sero, I.; Bisquert, J. Characterization of nanostructured hybrid and organic solar cells by impedance spectroscopy. *Phys. Chem. Chem. Phys.* **2011**, *13*, 9083–9118.

(28) Wang, Q.; Moser, J. E.; Gratzel, M. Electrochemical impedance spectroscopic analysis of dye-sensitized solar cells. *J. Phys. Chem. B* **2005**, *109*, 14945–14953.

(29) Koide, N.; Islam, A.; Chiba, Y.; Han, L. Y. Improvement of efficiency of dye-sensitized solar cells based on analysis of equivalent circuit. *J. Photochem. Photobiol., A* **2006**, *182*, 296–305.

(30) Wu, J.; Lan, Z.; Lin, J.; Huang, M.; Huang, Y.; Fan, L.; Luo, G.; Lin, Y.; Xie, Y.; Wei, Y. Counter electrodes in dye-sensitized solar cells. *Chem. Soc. Rev.* **2017**, *46*, 5975–6023.

(31) Boschloo, G.; Hagfeldt, A. Characteristics of the Iodide/Triiodide Redox Mediator in Dye-Sensitized Solar Cells. *Acc. Chem. Res.* **2009**, *42*, 1819–1826.

(32) Nelson, J. J.; Amick, T. J.; Elliott, C. M. Mass Transport of Polypyridyl Cobalt Complexes in Dye-Sensitized Solar Cells with Mesoporous TiO₂ Photoanodes. *J. Phys. Chem. C* **2008**, *112*, 18255–18263.

(33) Lee, S.-H. A.; Jackson, A.-M. S.; Hess, A.; Fei, S.-T.; Pursel, S. M.; Basham, J.; Grimes, C. A.; Horn, M. W.; Allcock, H. R.; Mallouk, T. E. Influence of Different Iodide Salts on the Performance of Dye-Sensitized Solar Cells Containing Phosphazene-Based Nonvolatile Electrolytes. *J. Phys. Chem. C* **2010**, *114*, 15234–15242.

(34) Giokas, P. G.; Miller, S. A.; Hanson, K.; Norris, M. R.; Glasson, C. R. K.; Concepcion, J. J.; Bettis, S. E.; Meyer, T. J.; Moran, A. M. Spectroscopy and Dynamics of Phosphonate-Derivatized Ruthenium Complexes on TiO₂. *J. Phys. Chem. C* **2013**, *117*, 812–824.

(35) Asbury, J. B.; Anderson, N. A.; Hao, E.; Ai, X.; Lian, T. Parameters Affecting Electron Injection Dynamics from Ruthenium Dyes to Titanium Dioxide Nanocrystalline Thin Film. *J. Phys. Chem. B* **2003**, *107*, 7376–7386.

(36) Kuang, D.; Ito, S.; Wenger, B.; Klein, C.; Moser, J.-E.; Humphry-Baker, R.; Zakeeruddin, S. M.; Grätzel, M. High Molar Extinction Coefficient Heteroleptic Ruthenium Complexes for Thin Film Dye-Sensitized Solar Cells. *J. Am. Chem. Soc.* **2006**, *128*, 4146–4154.

(37) Antila, L. J.; Myllyperkiö, P.; Mustalahti, S.; Lehtivuori, H.; Korppi-Tommola, J. Injection and Ultrafast Regeneration in Dye-Sensitized Solar Cells. *J. Phys. Chem. C* **2014**, *118*, 7772–7780.

(38) Clifford, J. N.; Palomares, E.; Nazeeruddin, M. K.; Gratzel, M.; Durrant, J. R. Dye dependent regeneration dynamics in dye sensitized nanocrystalline solar cells: Evidence for the formation of a ruthenium bipyridyl cation/iodide intermediate. *J. Phys. Chem. C* **2007**, *111*, 6561–6567.

(39) Feldt, S. M.; Wang, G.; Boschloo, G.; Hagfeldt, A. Effects of Driving Forces for Recombination and Regeneration on the Photo-voltaic Performance of Dye-Sensitized Solar Cells using Cobalt Polypyridine Redox Couples. *J. Phys. Chem. C* **2011**, *115*, 21500–21507.

(40) Safdari, M.; Lohse, P. W.; Häggman, L.; Frykstrand, S.; Högberg, D.; Rutland, M.; Asencio, R. A.; Gardner, J.; Kloo, L.; Hagfeldt, A.; Boschloo, G. Investigation of cobalt redox mediators and effects of TiO₂ film topology in dye-sensitized solar cells. *RSC Adv.* **2016**, *6*, 56580–56588.

(41) Yella, A.; Mathew, S.; Aghazada, S.; Comte, P.; Grätzel, M.; Nazeeruddin, M. K. Dye-sensitized solar cells using cobalt electrolytes: the influence of porosity and pore size to achieve high-efficiency. *J. Mater. Chem. C* **2017**, *5*, 2833–2843.

(42) Wang, J. C.; Violette, K.; Ogunsolu, O. O.; Cekli, S.; Lambers, E.; Fares, H. M.; Hanson, K. Self-Assembled Bilayers on Nanocrystalline Metal Oxides: Exploring the Non-Innocent Nature of the Linking Ions. *Langmuir* **2017**, *33*, 9609–9619.

(43) Ding, X.; Gao, Y.; Zhang, L. L.; Yu, Z.; Liu, J. H.; Sun, L. C. Visible Light-Driven Water Splitting in Photoelectrochemical Cells with Supramolecular Catalysts on Photoanodes. *ACS Catal.* **2014**, *4*, 2347–2350.

(44) Farnum, B. H.; Wee, K. R.; Meyer, T. J. Self-assembled molecular p/n junctions for applications in dye-sensitized solar energy conversion. *Nat. Chem.* **2016**, *8*, 845–52.

(45) Dilbeck, T.; Hill, S. P.; Hanson, K. Harnessing molecular photon upconversion at sub-solar irradiance using dual sensitized self-assembled trilayers. *J. Mater. Chem. A* **2017**, *5*, 11652–11660.